

## Article

# Effect of Mechanical Properties of Rail and Wheel on Wear and Rolling Contact Fatigue

Jung-Won Seo <sup>\*</sup>, Hyun-Moo Hur and Seok-Jin Kwon

Korea Railroad Research Institute, 176 Cheoldobakmulkwon-ro, Uiwang-si 16105, Gyeonggi-do, Korea; hmhur@krri.re.kr (H.-M.H.); jkwon@krri.re.kr (S.-J.K.)

\* Correspondence: jwseo@krri.re.kr; Tel.: +82-31-460-5210

**Abstract:** Rolling contact fatigue (RCF) and wear are important problems for the wheel and rail. RCF and wear is caused by contact stress and the slip ratio between the wheel and the rail. The material properties of the wheel and rail are an important factor to prevent the degradation caused by RCF and wear. In this study, the mechanical properties and fatigue characteristics of the two types of wheel and rail were evaluated, and the effects on wear and contact fatigue were examined. We found that the crack growth rate and the hardness were important factors in the contact fatigue and the wear. The rail steel with a higher crack growth rate and hardness had a low resistance to contact fatigue with large size damage. The hardness ratio and the total hardness are important factors in evaluating the wear resistance. In addition, we found that the residual stress increased proportionally to the maximum shear stress.

**Keywords:** railway; wear; rolling contact fatigue; crack growth



**Citation:** Seo, J.-W.; Hur, H.-M.; Kwon, S.-J. Effect of Mechanical Properties of Rail and Wheel on Wear and Rolling Contact Fatigue. *Metals* **2022**, *12*, 630. <https://doi.org/10.3390/met12040630>

Academic Editors: Riccardo Nobile and Zhengyi Jiang

Received: 25 February 2022

Accepted: 4 April 2022

Published: 6 April 2022

**Publisher's Note:** MDPI stays neutral with regard to jurisdictional claims in published maps and institutional affiliations.



**Copyright:** © 2022 by the authors. Licensee MDPI, Basel, Switzerland. This article is an open access article distributed under the terms and conditions of the Creative Commons Attribution (CC BY) license (<https://creativecommons.org/licenses/by/4.0/>).

## 1. Introduction

Railway vehicles play an important role as a means of mass transportation. Since static and dynamic forces are transferred through the interaction between the rail and the wheel, the small contact surface area between them undergoes the severest contact stress. Therefore, the interface between the rail and the wheel is exposed to various types of damage. The types of damage most frequently found on the contact surface of the wheel and rail are wear and rolling contact fatigue. Such damages can cause failures of the wheel and rail and could eventually lead to the derailment of railway vehicles, bringing great casualties and loss of property. Recently, as the speed and usage of railroad vehicles increase, the degradation of infrastructure is rapidly progressing, and the maintenance cost is also increasing. In particular, in order to predict rolling contact fatigue occurring in rails and remove cracks, periodic grinding should be carried out [1,2]. The typical rolling contact fatigue damage on rails is squats and head checks. Squats occur on the straight tracks, and head checks occur on the curved tracks. Recently, it is known that the white etching layer (WEL) generated by frictional heat during braking reduces the rolling contact fatigue life [3,4]. In the case of high-speed rail wheels, other types of rolling contact fatigue damage are occurring. This is local rolling contact fatigue (LRCF), which is different from the conventional rolling contact fatigue that occurs continuously [5,6]. Therefore, many researchers have examined ways to reduce damage occurring on the interface between the wheel and the rail [7–10]. Studies on the wheel and rail have been mostly conducted on the independent topics of the wear of the wheel/rail or of contact fatigue damages [11,12]. In addition, standards for the rail and wheels are specified independently, which does not include any provision for the wheel–rail interface [13,14]. However, damage such as wear and contact fatigue would occur on the interface between the wheel and the rail by rolling contact. Thus, wear and contact fatigue cannot be independent, but have a competitive relationship.

Razhkovskiy et al. [15] suggested an optimal ratio of the values of the hardness of the wheel and rail through their experiment to reduce wear. Wang et al. [16] investigated the contact fatigue and wear characteristics of the wheel and rail by changing the hardness of the wheel. They showed the wear of the wheel and rail linearly increased along with the increasing hardness of the wheel, and the damage mechanism shifted from adhesion wear to delamination wear. Hu et al. [17] investigated wear and contact fatigue according to the hardness ratio between the wheel and the rail. The rolling contact wear test was conducted while changing the hardness ratio of the rail to the wheel from 0.927 to 1.218. The wheel wear rate decreased dramatically at the hardness ratio of 1.128, and the rail wear rate showed a tendency to increase. Donzella et al. [18,19] proposed a model to evaluate wear and contact fatigue in the rail, and demonstrated a correlation between wear and contact fatigue through experiments. In addition, they showed that the plastic deformation and the residual stress induced by the repetitive rolling contact of the rail and wheel are important factors influencing on contact fatigue. Ishida [20] conducted contact fatigue tests to examine the relationship between contact fatigue damage and the residual stress. Batista [21] investigated the wear and evolution of residual stress by a repetitive contact fatigue test. Ueda et al. [22] investigated the effect of the carbon content and hardness of rail materials on contact fatigue through rolling contact tests. As the carbon content increased, the hardness increased, and plastic deformation at the contact surface was suppressed. Accordingly, the depths of cracks and the numbers of spalls occurring at the contact surface were reduced. Studies have been conducted to evaluate the effect of metal structures on wear and contact fatigue [23,24]. Liu et al. [23] conducted a rolling contact test under various load conditions to investigate the relationship between microstructure and wear mechanism. At high contact pressure, severe plastic deformation occurred, resulting in fatigue wear, and at low contact pressure, adhesive wear occurred. As the contact pressure increased, the occurrence of fatigue cracks gradually increased. Pereira et al. [24] evaluated the effect of contact fatigue on rail steels with spheroidized pearlite and fully pearlitic microstructures. It was shown that steel with spheroidized pearlite reduced the occurrence of contact fatigue cracks more than that in the fully pearlitic microstructure.

Recently, many studies have been conducted on the wear and contact fatigue characteristics of bainitic steel [25–28]. Li et al. [25] investigated the effect of upper bainite microstructure on wear in high-speed rail wheels, and Liu et al. [26] performed rolling/sliding wear tests under various conditions using bainitic rail steel. The bainitic rail steel showed that the plastic deformation and wear mechanism were changed by the contact pressure and slip rate. Miranda et al. [27] and Liu et al. [28] investigated the effects of wear and contact fatigue on materials with the same chemical composition and hardness but with pearlitic and bainitic microstructures. The results revealed that the microstructure had a significant role in wear and contact fatigue damage. The bainitic microalloyed steel showed lower wear rates and greater resistance to contact fatigue than the pearlitic one. The studies conducted so far have investigated the surface hardness, the residual stress, and the microstructure as factors causing wear or contact fatigue. In the case of using the generally employed shakedown map to evaluate contact fatigue, the only material property of shear yield strength is used [29]. However, since the factors causing wear and contact fatigue are various and interrelated with each other, an assessment derived from single value of material property could be unreasonable. In addition, the relationship between the contact fatigue and wear of the wheel and rail should be clearly identified, but such research is insufficient.

The assessment and prediction of the wear and the contact fatigue of the rail and wheel are important for the safe service and maintenance of railway vehicles. Among the factors affecting the wear and the contact fatigue of the wheel and rail are the fracture toughness and the fatigue crack grow rate. In this study, the mechanical properties and fracture toughness characteristics of the two types of rails and wheels were evaluated, and the effects of the mechanical property on the wear and contact fatigue were examined by

conducting rolling contact fatigue tests. In addition, the evolution of residual stress under various loading conditions were examined.

## 2. Mechanical Properties

### 2.1. Materials

The KS60-rail and UIC60-rail and the RSW-wheel and R7-wheel were used for the test conducted in this study. The KS60-rail and RSW-wheel are generally used on the main line of the rail network in Korea, whereas the UIC60-rail and R7-wheel are used for the high-speed railway. Tables 1 and 2 show the chemical compositions of the materials of the wheel and rail steels, respectively. The UIC60-rail contains a greater carbon component than the KS60-rail, and the components of Al and N are additionally added thereto. The RSW-wheel also contains a greater carbon component than the R7-wheel, and the components of Cu, Mo, Ni, V, etc. are additionally included in the R7-wheel.

**Table 1.** Chemical composition of rail steel (wt.%).

Steel	C	Si	Mn	P	S	Al	N
KS60	0.63–0.75	0.15–0.30	0.70–1.10	0.030	0.025		
UIC60	0.65–0.82	0.13–0.60	0.65–1.25	0.030	0.008–0.030	0.004	0.009

**Table 2.** Chemical composition of wheel steel (wt.%).

Steel	C	Si	Mn	P	S	Cr	Cu	Mo	Ni	V	(Cr+Mo+Ni)
RSW	0.67	0.15	0.6–0.8	0.045	0.045	0.35					
R7	0.52	0.40	0.80	0.035	0.035	0.30	0.30	0.08	0.30	0.05	0.50

Figure 1 shows the heat treatment process of a typical railroad vehicle wheel [30]. The wheel heat treatment is carried out to increase the hardness of the contact surface that is in rolling contact with the rail and to generate compressive residual stress. As for the heat treatment method, tempering is performed after quenching the contact surface. As shown in Figure 1b, the heating temperature before quenching is about 850 °C, and it is rapidly cooled to a temperature below 300 °C through water cooling on the contact surface. Tempering is performed to stabilize the microstructure; the tempering temperature is about 520 °C and the tempering time is about 6 h. Detailed heat treatment conditions are set differently for each wheel manufacturer. Figure 2 shows the microstructure of the wheel and rail. Wheels and rails have different microstructures. Figure 2a shows the microstructure of the R7-wheel, which is typical of pearlite and ferrite of carbon steel. The white part in the picture is ferrite, and the black part is pearlite. Figure 2b shows the microstructure of the RSW-wheel, which is similar to that of the R7-wheel. Figure 2c shows the microstructure of the UIC60-rail, and it is composed of pearlite. Figure 2d shows the microstructure of the KS60-rail, similar to that of the UIC60-rail.

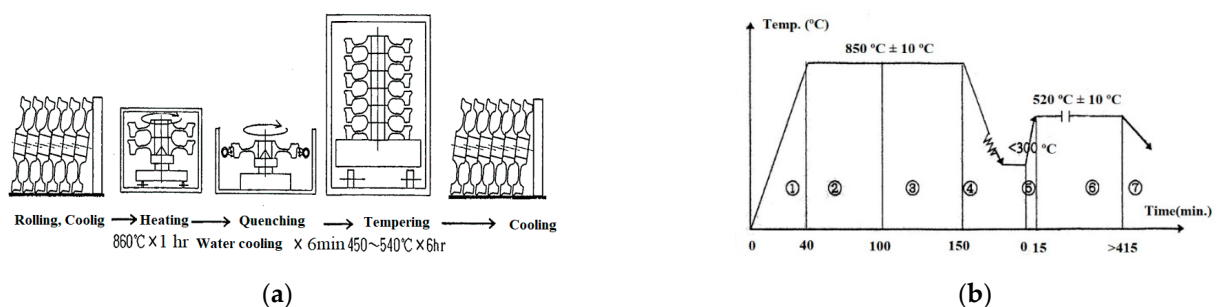


**Figure 1.** Manufacturing process of the wheel: (a) heat treatment process; (b) temperature variation.

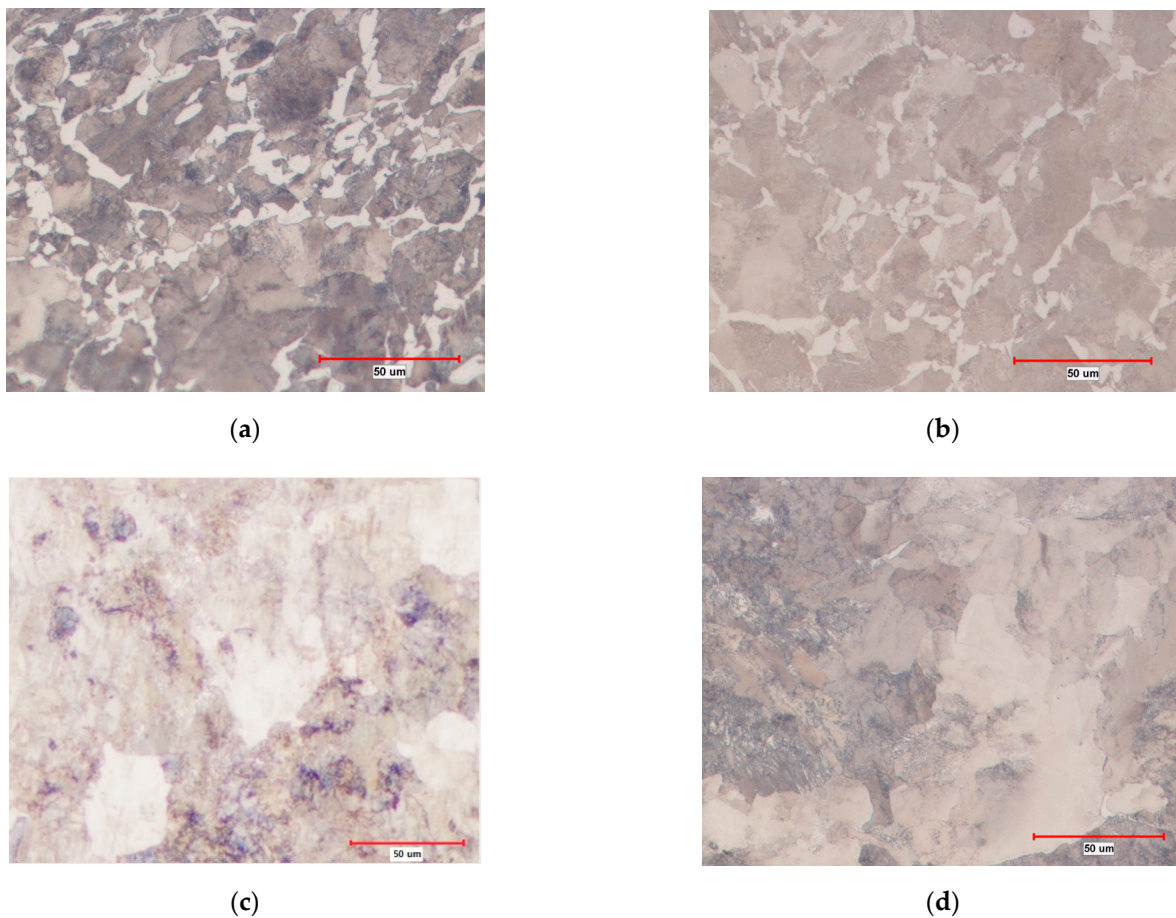


**Figure 2.** Microstructure of wheels and rails: (a) R7-wheel; (b) RSW-wheel; (c) UIC-rail; (d) KS60-rail.

## 2.2. Tensile and Hardness Test

### 2.2.1. Test Method

Figure 3 shows the specimen configuration for the tensile test, and the gauge diameter was 9 mm. The tensile tests were conducted according to the ASTM E-8. The hydraulic tester of 250 kN capacity was employed for the tensile test, and the COD gauge (Shimadzu, Kyoto, Japan) and DAQ equipment (Shimadzu, Kyoto, Japan) were used to measure the datum of real-time displacement and load.

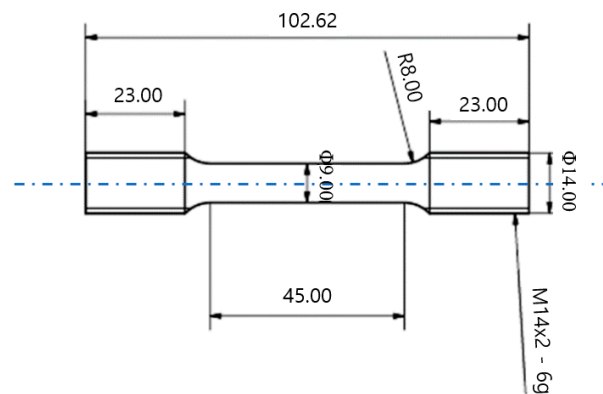


**Figure 3.** Specimen configuration for tensile test.

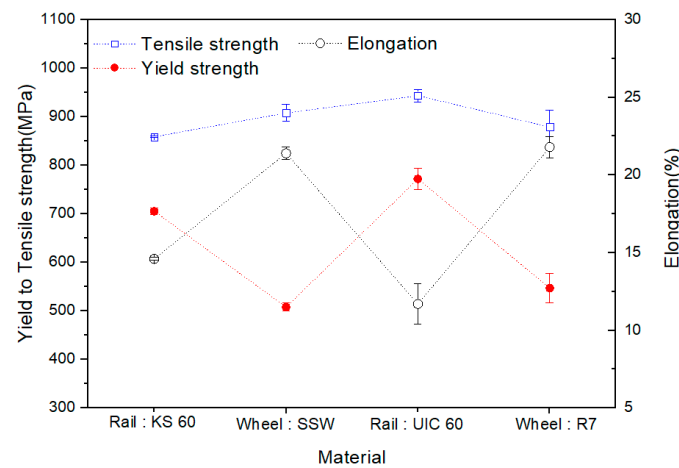
### 2.2.2. Test Results

Table 3 shows the results of the tensile test, and Figure 4 illustrates a comparison between the test results of wheel and rail specimen. The tensile strength of each material

appeared similar to each other. However, the yield strength of the materials of wheel and rail reveal a significant difference. The yield strength of the KS60-rail and UIC60-rail appeared higher than that of the RSW-wheel and R7-wheel. However, the elongation represents the trend opposite to the yield strength. The higher yield strength of material accompanied the corresponding lower of elongation, and thereby, the elongation of the wheel appeared higher than that of the rail. Figure 5 shows the hardnesses of the rail and wheel. The hardness of the rail appeared higher than that of the wheel. The UIC60-rail had the highest hardness, greater than that of the KS60-rail. From the results obtained from the hardness test, the KS60-rail was predicted to wear more than the UIC60-rail.

**Table 3.** Tensile test results.

Steel	Yield Strength (MPa)	Ultimate Strength (MPa)	Elongation (%)
KS60	706	859	15
RSW	508	908	21
UIC60	772	943	12
R7	547	879	22



**Figure 4.** Comparison of yield and tensile strength by wheel and rail steel.

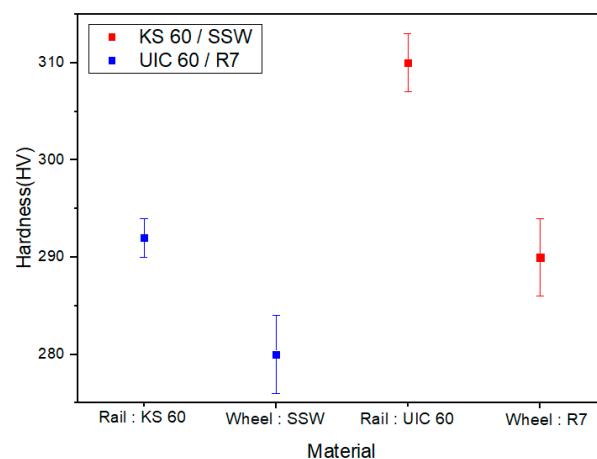


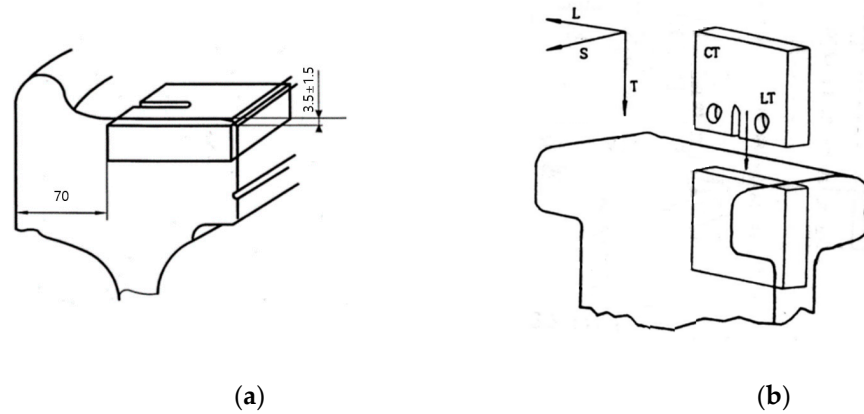
**Figure 5.** Comparison of hardness by wheel and rail steel.

### 2.3. Fatigue Crack Growth Test

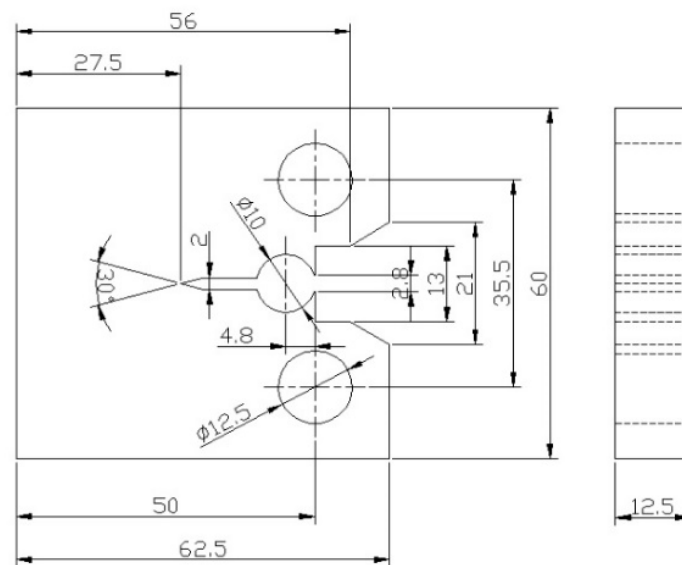
#### 2.3.1. Test Method

Figure 6 shows the sampling locations of crack propagation test specimens and fracture toughness specimens. Test specimens for the tests of fracture toughness and fatigue crack

growth rate were taken from the center of the head of the rail and from the rim of the wheel. The crack in the rail specimen grew downward, while the crack in the wheel specimen grew circumferentially. Figure 7 shows the shapes and dimensions of the crack propagation specimens. The widths and thicknesses of the specimens were 60 mm and 12.5 mm, respectively.



**Figure 6.** Orientation of fracture toughness and crack growth specimens: (a) wheel; (b) rail.



**Figure 7.** Specimen configuration for crack growth rate test.

The crack growth tests were conducted according to ASTM E647. On the tip of the notch of the test specimen prepared for the crack growth test, the preliminary crack was inserted to the point of  $a/W = 0.5$  by applying the fatigue load. The load ratio  $R = 0.1$  was applied to the test with a test speed of 10Hz. The  $da/dN-\Delta K$  curve was obtained from Equation (1) [31].

$$K = \frac{\Delta P}{B\sqrt{W}} \frac{(2 + \alpha)}{(1 - \alpha)^{3/2}} f(\alpha) \quad (1)$$

$$f(\alpha) = 0.886 + 4.64\alpha - 13.31\alpha^2 + 14.72\alpha^3 - 5.6\alpha^4 \quad (2)$$

where  $\Delta P$  is the difference between the maximum load and the minimum load;  $B$ ,  $a$ ,  $W$  represent the thickness of the test specimen, crack length, width of test specimen, respectively; and  $\alpha$  is  $a/W$ .

### 2.3.2. Test Results

Figure 8 shows the results of the crack growth rate test of wheel and rail materials. The crack growth parameters of  $C$  and  $m$  (Paris' law) were obtained from Figure 8 and summarized in Table 4. As illustrated in Figure 4, the crack growth characteristics of the materials of the wheel and rail appeared similar except for the case of small values of  $\Delta K$ . The EN 13674 [13] presents criteria for the crack growth rate of the rail material. Those were 17 m/Gc and 55 m/Gc, corresponding to the values of  $\Delta K$  of 10 MPa $\sqrt{m}$  and 13.5 MPa $\sqrt{m}$ . Figure 9 represents a comparison of the crack growth rate of wheel and rail that satisfy the requirement of the EN standard. As shown in Figure 9, the crack growth rate of the rail appears higher than that of the wheel. The UIC60-rail had the highest value of the crack growth rate, 17.5 m/Gc at the  $\Delta K$  of 13.5 MPa $\sqrt{m}$ . The UIC60-rail revealed the highest yield strength with the lowest elongation. Figure 10 represents the relationship ( $a-N$ ) between the cycles and crack length in the rail. It is difficult to distinguish the crack growth rate from the results of the crack growth test illustrated in Figure 8. However, the  $a-N$  curve plotted in Figure 10 shows the crack growth rate distinguished clearly. The UIC60-rail had a higher crack growth rate than that of the KS60-rail.

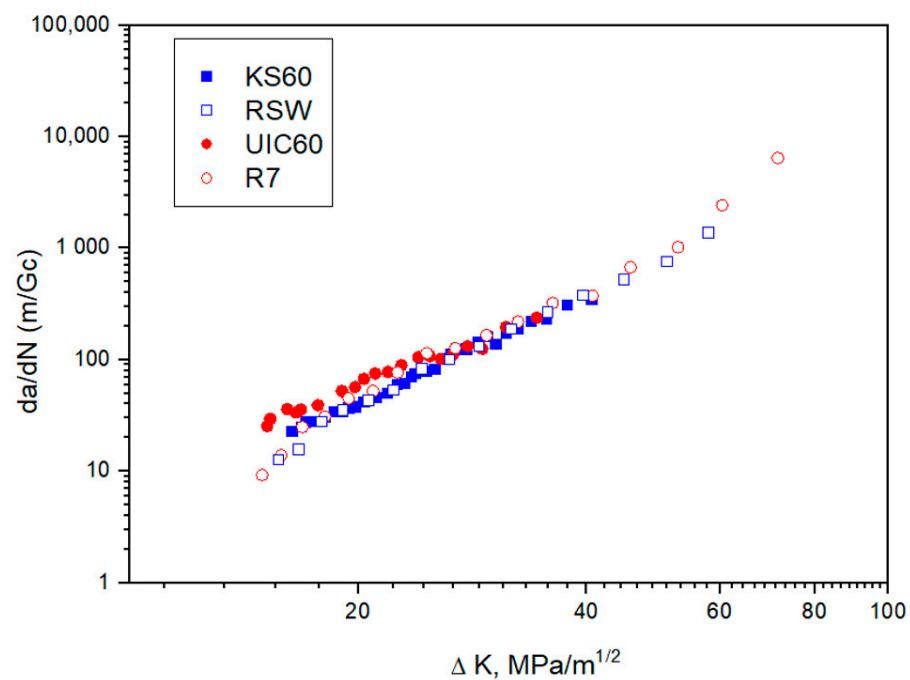


Figure 8. Fatigue crack growth rate test results.

Table 4. FCGR characterizing parameters.

Specimen No.	$C$	$m$	$\Delta K$ (MPa $\sqrt{m}$ )	$da/dN$ (m/Gc *)	$\Delta K$ (MPa $\sqrt{m}$ )	$da/dN$ (m/Gc *)
KS 60	$3.3 \times 10^{-3}$	3.21	10	5.37	13.5	14.07
RSW	$1.4 \times 10^{-3}$	3.41	10	3.55	13.5	9.87
UIC 60	$1.3 \times 10^{-2}$	2.78	10	7.59	13.5	17.47
R7	$6.9 \times 10^{-4}$	3.66	10	3.16	13.5	9.49

\* Gc = 1E9 cycle.

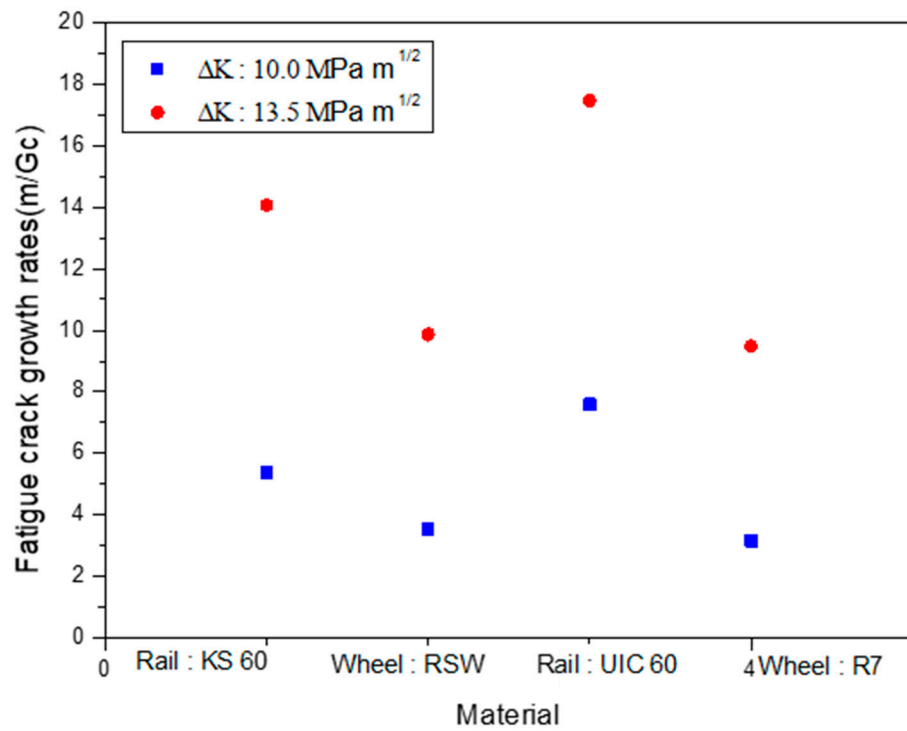


Figure 9. Comparison of fatigue crack growth rate.

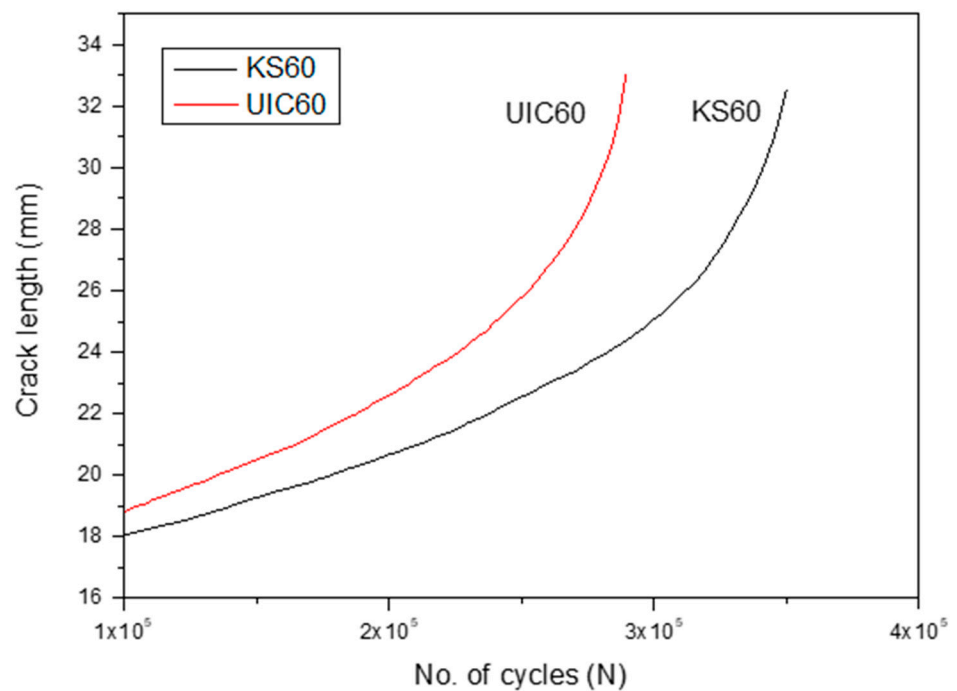
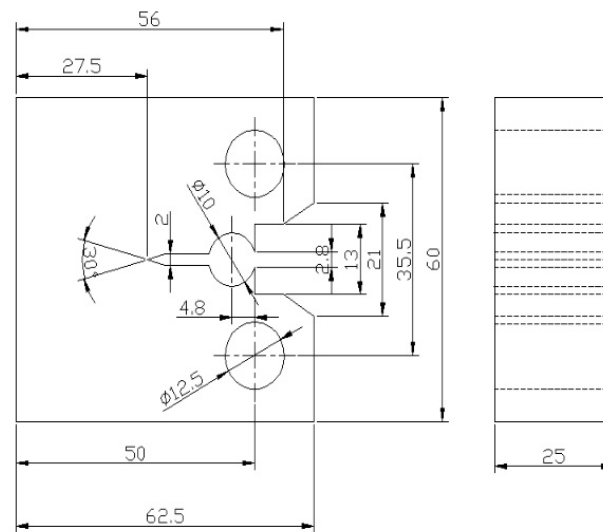


Figure 10. Cycles vs. crack length in rail steel.

#### 2.4. Fracture Toughness Test

##### 2.4.1. Test Method

Figure 11 shows the shapes and dimensions of the fracture toughness specimens. The widths and thicknesses of the specimens were 60 mm and 25 mm, respectively. The fracture toughness test of the materials was carried out according to ASTM E339.



**Figure 11.** Specimen configuration for fracture toughness test.

#### 2.4.2. Test Results

Figure 12 illustrates a comparison of the fracture toughnesses of the rail and wheel. In the case of the KS60-rail and RSW-wheel, the fracture toughness of the rail appeared higher than that of the wheel. In the case of the UIC60-rail and R7-wheel, the fracture toughness of the wheel appeared higher than that of the rail. In addition, since the fracture toughness of the UIC60 rail was the lowest and that of the R7 wheel was the highest, the fracture toughness difference between the two materials was large. The fracture toughness of the KS60-rail was  $73 \text{ MPa}\sqrt{\text{m}}$ , 1.8 times higher than  $41 \text{ MPa}\sqrt{\text{m}}$  of the fracture toughness of the UIC60-rail. The fracture toughness of the RSW-wheel was  $63 \text{ MPa}\sqrt{\text{m}}$ , whereas it was  $82 \text{ MPa}\sqrt{\text{m}}$  for the R7-wheel, 1.3 times higher than that of the RSW-wheel.

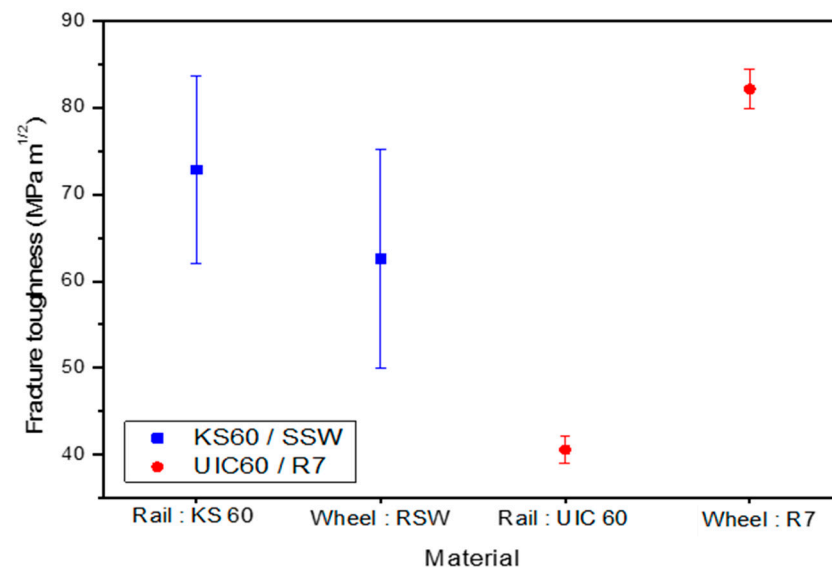


**Figure 12.** Comparison of fracture toughness by wheel and rail steel.

### 3. Wear and Contact Fatigue Test

#### 3.1. Test Apparatus

The twin-disc tester was used to evaluate the wear and the contact fatigue characteristics of wheel and rail. Figure 13 shows a schematic diagram of the twin-disc tester. The test machine was equipped with two independent motors controlling the speed of rotation, and the hydraulic unit attached thereto was designed to apply the load to the test specimen.

The slip ratio could be controlled by adjusting the rotational speed of the shafts. The test conditions of applying the load, rotational speed, and slip ratio were fully controlled by a computer, and all of the data collected during the test were saved.

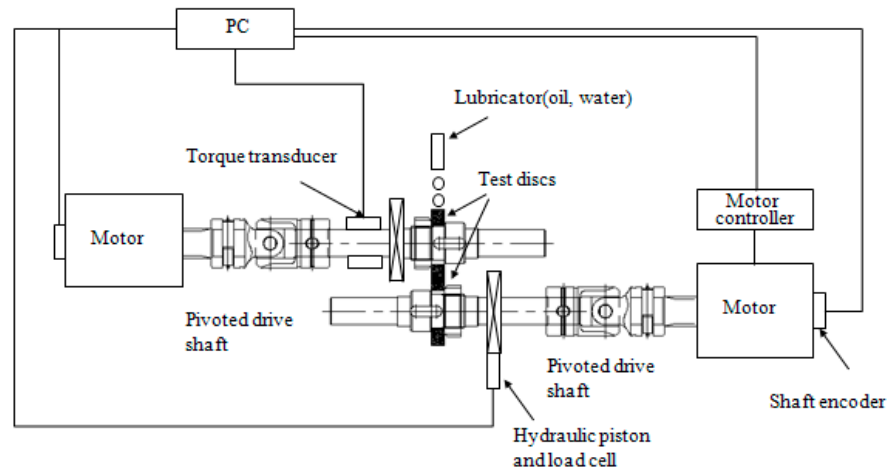


**Figure 13.** Schematic diagram of the twin-disc test machine.

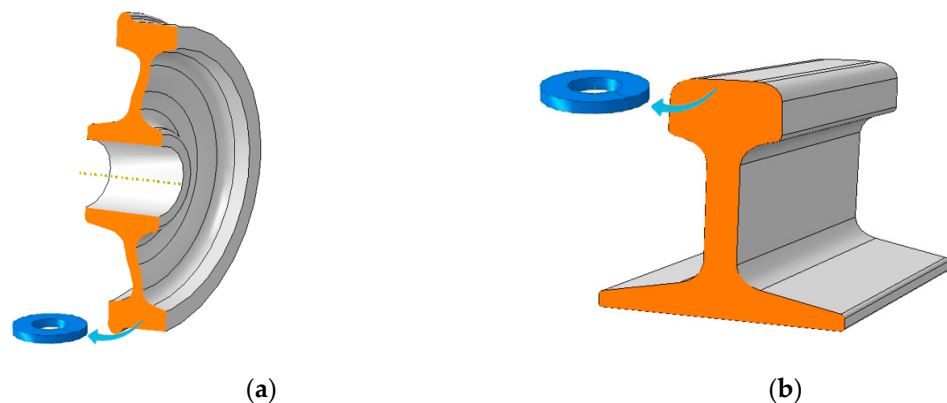
### 3.2. Specimen and Test Methodology

Figure 14 shows the location of the rolling contact test specimen. The wheel specimens were cut from the rim of a wheel, and the rail specimens were cut from the head of a rail. Both the wheel and rail test pieces were taken from the position as close as possible to the contact surface. Figure 15 shows the shape of the rolling contact test piece, and both wheel and rail test pieces had the same shape and dimensions. The diameters and widths of the specimens were 50 mm and 10 mm, respectively. The roughness of the contact surface was ground to about  $0.3 \mu\text{m}$  to simulate the roughness of the wheel and rail. The maximum contact pressure  $P_0$  was calculated using Equations (3) and (4) [32].

$$P_0 = 0.418 \left[ \frac{(PE)}{LR} \right]^{1/2} \quad (3)$$

$$\frac{1}{R} = \frac{1}{R_w} + \frac{1}{R_r} \quad (4)$$

where  $P$  is the applied load,  $E$  is Young's modulus,  $L$  is the specimen width, and  $R_r$  and  $R_w$  are the radii of the rail and wheel specimens, respectively.



**Figure 14.** Location and orientation of the test specimen: (a) wheel; (b) rail.

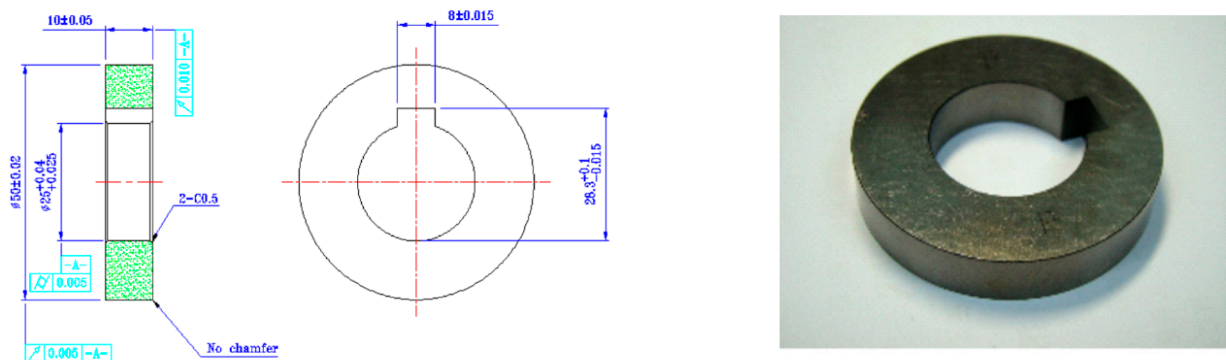


**Figure 15.** Shape and dimensions of rolling contact specimen.

For the wear test, the contact stress, the slip ratio, and the rotation speed were set at 1500 MPa, 1.5%, and 500 rpm, respectively. The wear tests were performed until the number of rotations reached  $2 \times 10^5$  cycles. The mass changes in the specimens were weighed by an electric weighing scale with a resolution of 0.00001 g. For the contact fatigue test, the contact stress, slip ratio, and rotation speed were also set at 1500 MPa, 1.5%, and 500 rpm, respectively. The test machine was set to stop after every 10,000 cycles to observe the progress of the damage on the surface through a microscope. In the wear test and the contact fatigue test, three specimens were used, respectively, according to the type of test.

### 3.3. Wear Test Results

Figure 16 shows the results of the wear test. The wear rate ( $\mu\text{g}/\text{m}/\text{mm}^2$ ) was calculated by dividing the volume of wear loss by the rolling distance and contact area. The RSW-wheel exhibited the largest wear rate, whereas the smallest wear rate was exhibited by the material used for the UIC60-rail. Both types of test specimens commonly exhibited a larger wear rate in the materials used for the wheel than those used for the rail. This was attributable to the hardness of the rail being higher than that of the wheel.

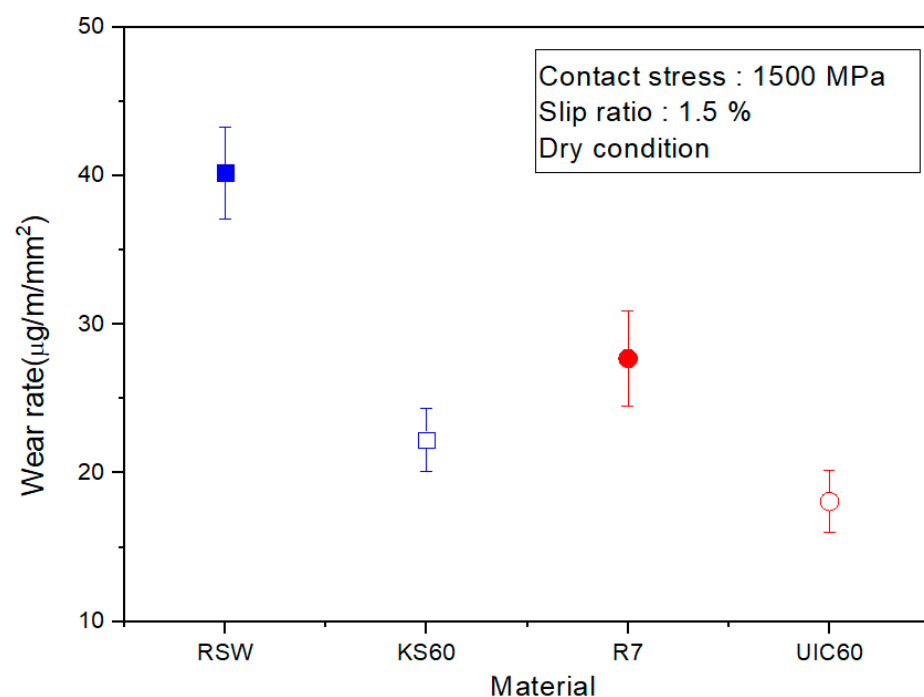


**Figure 16.** Comparison of wear rate of wheel and rail.

## 4. Discussion

### 4.1. Hardness and Wear

Figure 17 shows the total wear rate (the sum of the wear rate of the rail and the wheel) and the wear rate difference (the difference between the wear rates of the rail and the wheel). The cases of the wheel and rail that employed materials resistant to wear commonly showed a small total wear rate with less wear rate difference. In the case of the pair of the KS60-rail and RSW-wheel, the total wear rate was  $62 \mu\text{g}/\text{m}/\text{mm}^2$  and yielded a wear rate difference of  $18 \mu\text{g}/\text{m}/\text{mm}^2$ . The case of the pair of the UIC60-rail and R7-wheel rendered a total wear rate of  $46 \mu\text{g}/\text{m}/\text{mm}^2$  with a wear rate difference of  $10 \mu\text{g}/\text{m}/\text{mm}^2$ . These results show the pair of UIC60-rail and R7-wheel had a higher wear resistance than that of the pair of the KS60-rail and RSW-wheel.

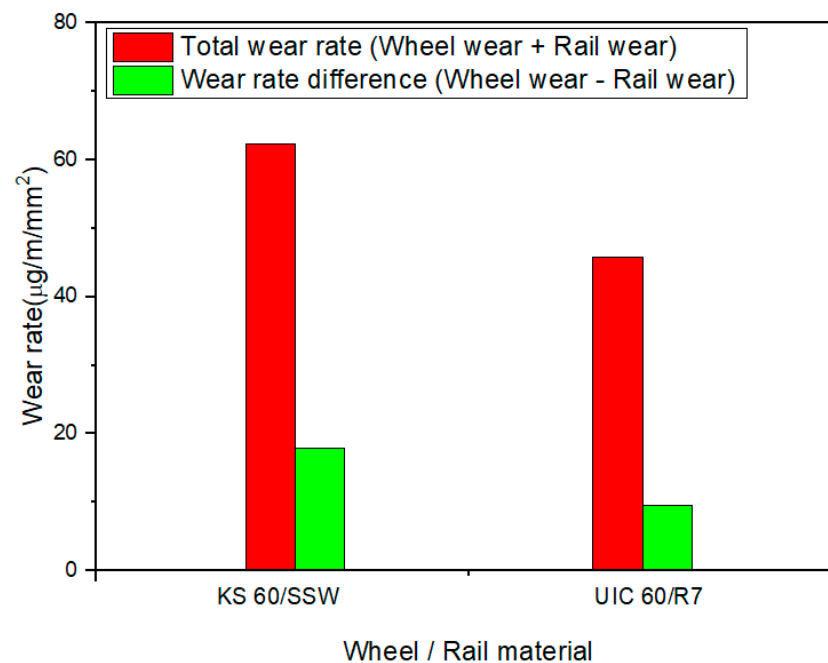


Figure 17. Total wear rate and difference.

The mechanical property of materials most influential on wear is the surface hardness. The wear resistance of the materials used for the wheel and rail is evaluated by using the hardness ratio (rail hardness/wheel hardness) [15,33]. Figure 18 shows the hardness ratios of test specimens and the total hardnesses (rail hardness + wheel hardness). In the test conducted in this study, the hardness ratio of the materials used for the wheel and rail respectively did not exhibit a significant difference, while the total hardness had a large difference. Therefore, as illustrated in Figure 17, the wear rate of the materials of large total hardness used for the UIC60-rail and R7-wheel decreased. As in the case of the test conducted in this study, which exhibited a similar hardness ratio with a large difference in the total hardness of the materials, the evaluation of the wear resistance of materials by relying solely on the hardness ratio becomes difficult. Figure 19 shows a comparison between the total hardness and the wear rate with the data from the reference [15]. As illustrated in the Figure 13, the total hardness and the total wear rate decreased linearly. Therefore, the evaluation of wear resistance by relying on the two factors of the hardness ratio and the total hardness seems desirable.

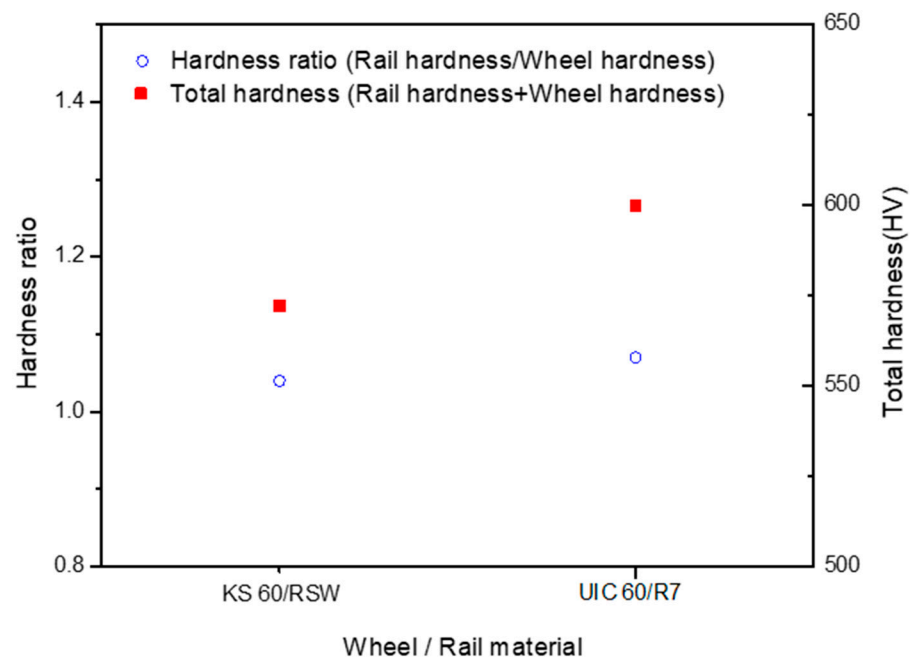


Figure 18. Hardness ratio and total hardness.

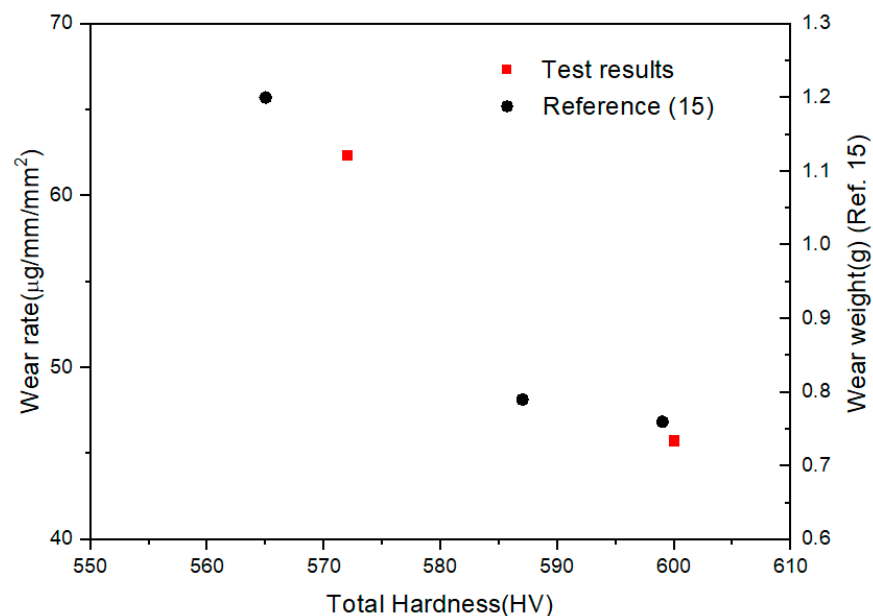


Figure 19. Relationship between total hardness and wear.

#### 4.2. Fracture Toughness and Contact Fatigue

Figure 20 shows the results of the contact fatigue test of the wheel and rail. In general, in the contact fatigue test the damage usually formed as pitting or spalling. In this study, the contact fatigue damage occurred on the surface of the rail specimen. Figure 21 shows cracks and microstructures in the wheels and rails. The microstructure of the contact surface was deformed by vertical and traction forces. Cracks originated from the surface and propagated along the deformed microstructure. The contact fatigue life of the pair of KS60-rail and RSW-wheel appeared 1.4 times longer than that of the pair of the UIC60-rail and R7-wheel. The result is opposite to that obtained from the wear test. In the wear test, the wear resistance of the pair of the UIC60-rail and R7-wheel was better than that of the pair of the KS60-rail and RSW-wheel. When the plastic deformation of materials

by the cyclic contact load exceeded the critical shear strain, wear and contact fatigue damage occurred. Table 3 shows the yield strength and the elongation of the KS60-rail and UIC60-rail, respectively. Since the KS60-rail has lower yield strength with a higher elongation than that of the UIC60-rail, plastic deformation is more probable, with more wear owing to the material exceeding the critical value. Zhou et al. [34] conducted the wear and contact fatigue tests of the four materials of different carbon contents used for rail. They reported that materials with high carbon content had increased wear resistance as the hardness increased. However, as the hardness increased, the notch sensitivity factor of the material increased, and the fatigue resistance decreased due to a gradual transition from a wear-dominant mechanism to a fatigue-dominance mechanism. These results correspond to those obtained from the test conducted in this study.

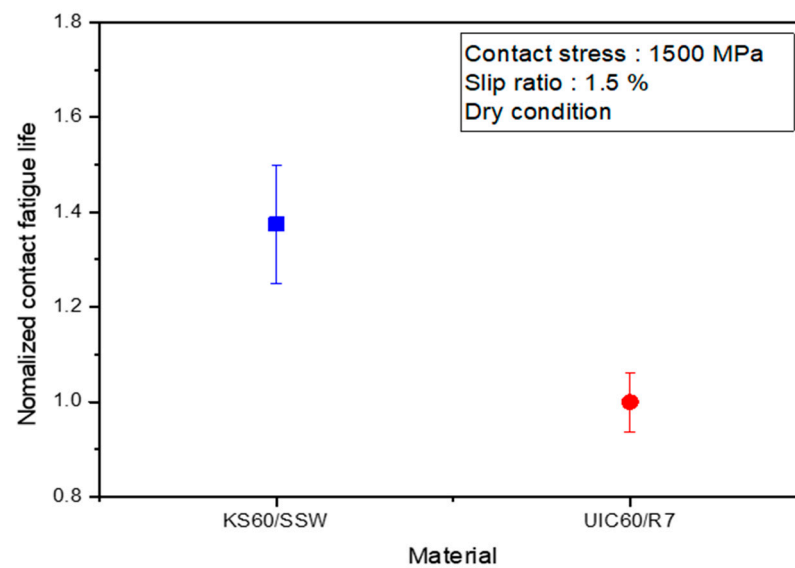
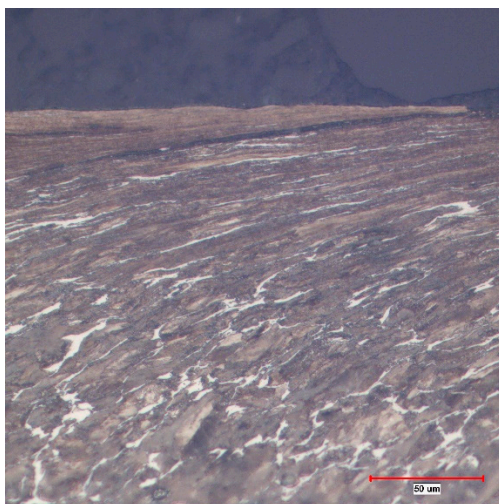
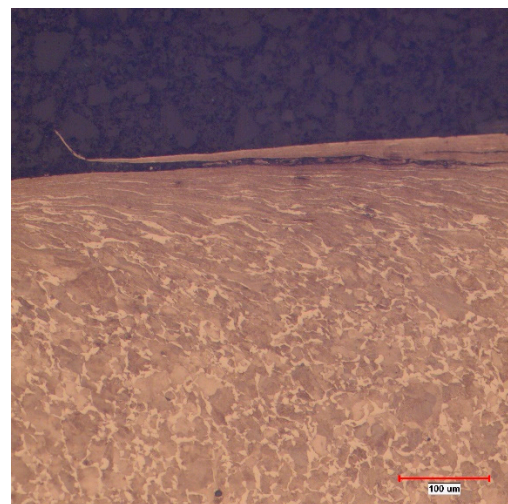


Figure 20. Contact fatigue test results.



(a)



(b)

Figure 21. Microstructure and cracks generated on the surfaces of wheel and rail specimens: (a) wheel specimen (R7); (b) Rail specimen (UIC60).

The fracture toughness and the crack growth rate of materials are factors affecting materials with fatigue and failure. The fracture toughness represents the fracture resistance to critical cracks, whereas the crack growth rate represents the resistivity to crack growth.

Figure 22 shows the fracture toughness and the crack growth rate of the two materials used for rail. The fracture toughness of the KS60-rail appeared higher than that of the UIC60-rail, whereas the crack growth rate appeared smaller than that of the UIC60-rail. Therefore, as illustrated in Figure 20, the contact fatigue life of the KS60-rail appeared longer than that of the UIC60-rail. Figure 23 shows the surface of a specimen that completed the contact fatigue test. The size of the surface damage of the UIC60-rail appeared larger than that of the KS60-rail. Since the mechanical property of the KS60-rail is rather ductile, that caused pitting on its surface easily; however, the pitting did not grow further owing to the larger amount of wear. On the contrary, the UIC60-rail showed a faster crack growth owing to its lower fracture toughness and higher hardness, which rendered less wear and eventually resulted in a surface damage larger than that of the KS60-rail. Such interaction between wear and contact fatigue corresponds to the experimental results reported by Donzella et al. [18,19].

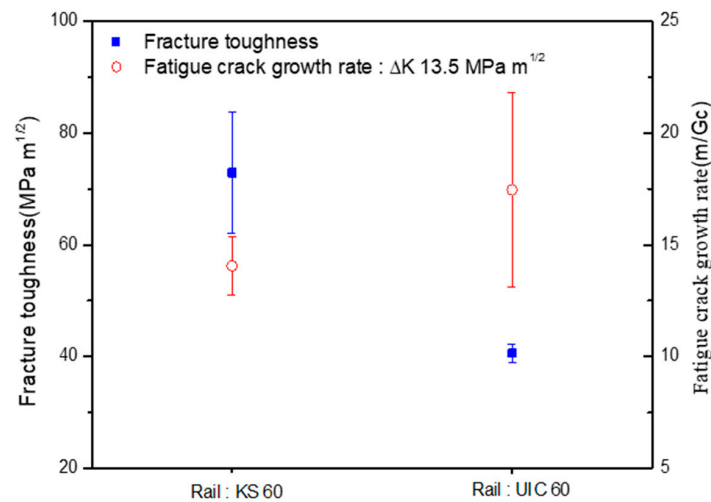


Figure 22. Comparison of fracture toughness and fatigue crack growth rate.

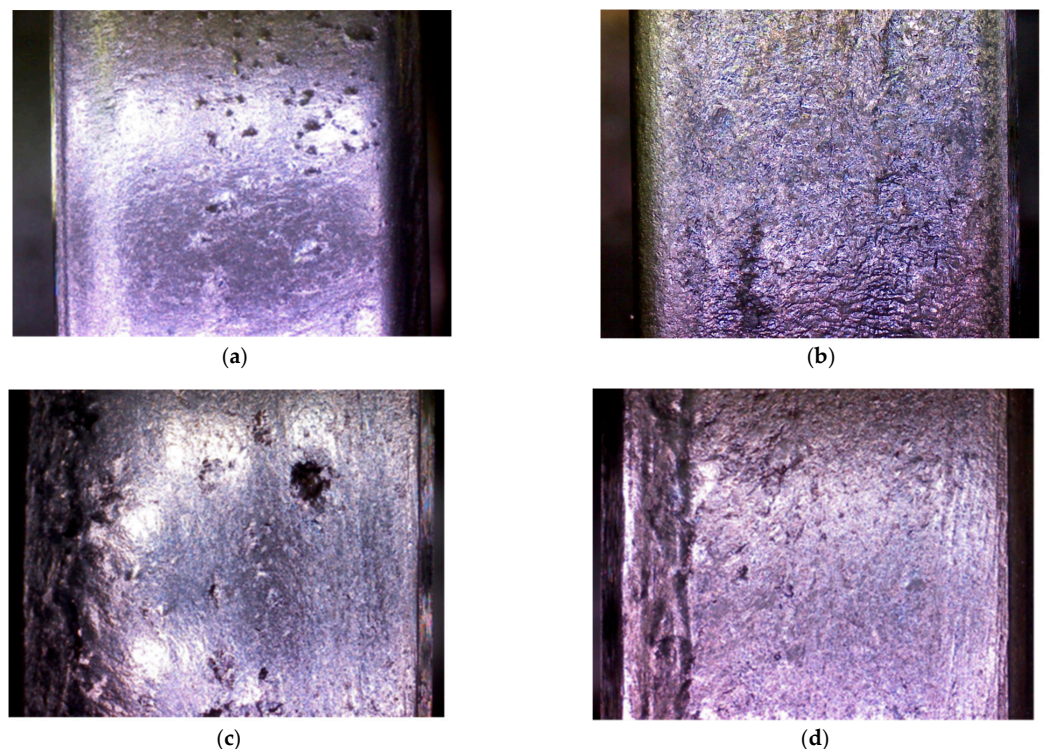


Figure 23. Wheel and rail surface condition after fatigue test: (a) Rail: KS 60; (b) Wheel: RSW; (c) Rail: UIC 60; (d) Wheel: R7.

The wear and the contact fatigue of the wheel and rail are not results that develop independently; they are results of the interaction between them. Therefore, an assessment of the surface damage of the wheel or rail needs to take the fracture toughness and the crack growth rate into account as well as mechanical properties such as the hardness and torsional shear strength [35].

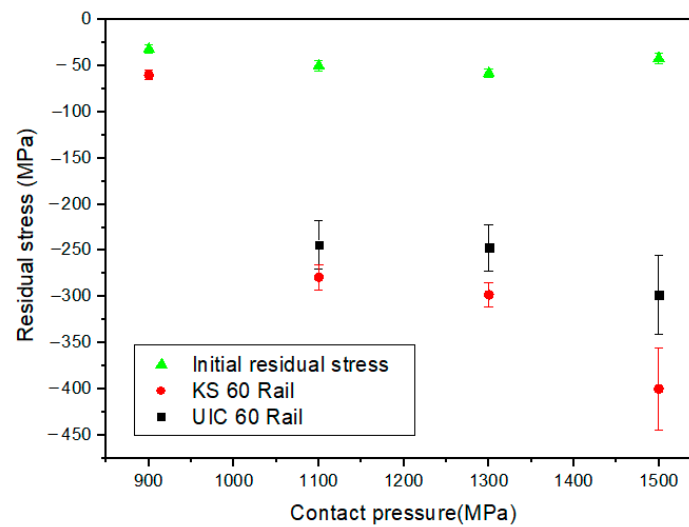
#### 4.3. Residual Stress Evolution

Railway vehicles run by the repetitive rolling contact of the wheel and rail. When the contact stress exceeds the elastic limit by the first loading, the plastic deformation of the contact surface between the wheel and rail occurs and the residual stress is created. The residual stress created by the rolling contact varies according to the axle load, coefficient of friction, and tractive force. In this study, the residual stress evolution according to various contact conditions was examined. The residual stress in the wheel and rail is an important factor, because it affects either the rail or wheel with crack initiation, and it gives us information about the history of the loading applied to the contact surface. The initial residual stress before the beginning of the rolling contact test and the residual stress after tests were measured. The surface residual stress was measured through the X-ray method and is illustrated in Figure 24.



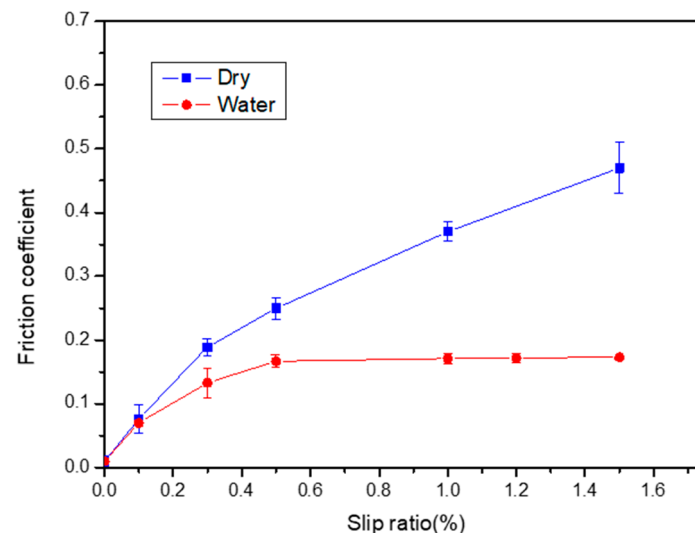
**Figure 24.** Residual stress measurement.

Figure 25 shows the variation in the residual stress according to the contact stress. In accordance with the increase in contact stress, the residual stress increased. With the increase in the contact stress, the plastic deformation also increased and the residual stress increased. In Figure 25, the residual stress created in the KS60-rail was larger than that in the UIC60-rail. This was due to the lower yield strength and the larger elongation of the KS60-rail than that of UIC60-60, which promoted the plastic deformation resulted in the larger residual stress.



**Figure 25.** Residual stress variation according to contact stress.

The vertical load as well as the tractive force affect the rail and wheel with residual stress. Thus, the tests were conducted by changing the slip ratio to examine the residual stress in the KS60-rail in accordance with the tractive force. Water was used as a lubricant by taking the frictional coefficient varying in accordance with the lubrication. Figure 26 shows the friction coefficient variation under the dry and the water conditions. Under the dry condition without lubrication, the frictional coefficient increased proportionally to the increasing slip ratio, and it was 0.47 at the 1.5% of the slip ratio. Under the water condition, the friction coefficient was 0.17 at 0.5% of the slip ratio, showing a significant difference from that of the dry condition. However, the friction coefficient did not show a significant change after 0.5% of the slip ratio.



**Figure 26.** Friction coefficient variation according to slip ratio.

Figure 27 shows the residual stress variation according to the slip ratio. The residual stress in the initial test specimen was  $-50$  MPa, and according to the increasing slip ratio, the residual stress increased under both the dry and the water conditions. Under the water condition, the residual stress was  $-200$  MPa at 1.5% of the slip ratio, whereas it was  $-400$  MPa at the same level of the slip ratio under the dry condition. The friction coefficient was associated with the tractive force of the wheel and rail. The tractive force increased proportionally to the friction coefficient. Therefore, the larger tractive force was generated

in the dry condition and resulted in a residual stress larger than that which resulted in the water condition.

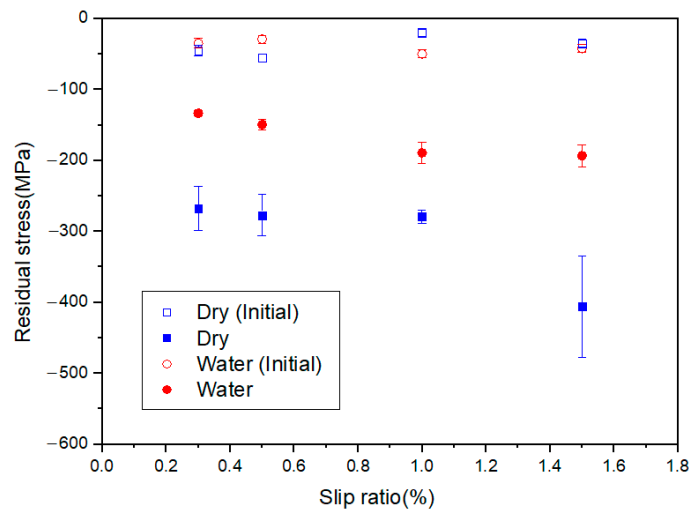


Figure 27. Residual stress variation according to slip ratio.

The contact fatigue damage to the wheel and rail can be explained by employing the maximum shear stress [36,37]. The fatigue index for predicting the contact fatigue life for cracks occurring on the surface can be expressed by Equation (5) [36,37]. The maximum shear stress can be expressed by Equation (6) using the maximum contact pressure and friction coefficient [36,37]. Figure 28 illustrates the relationship between the maximum shear stress and the residual stress. The linear relationship between the maximum shear stress and the residual stress is shown, and it is expressed by Equation (7).

$$FI_{surf} = f - \frac{k}{P_0} > 0 \tag{5}$$

$$\tau_{max} = \mu P_0 \tag{6}$$

$$\sigma_r = -0.45\tau_{max} - 96.85 \tag{7}$$

where  $FI_{surf}$  is the fatigue index,  $f$  is the traction coefficient,  $\mu$  is the friction coefficient,  $P_0$  is the maximum contact pressure,  $k$  is the shear yield strength,  $\tau_{max}$  and  $\sigma_r$  are the maximum shear stress and the residual stress, respectively.

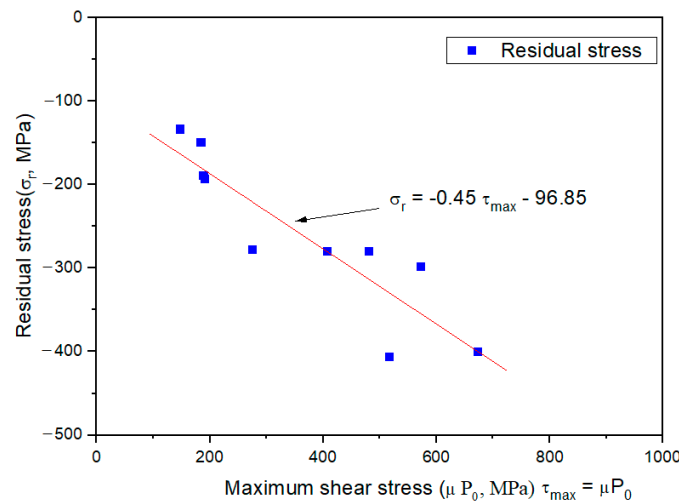
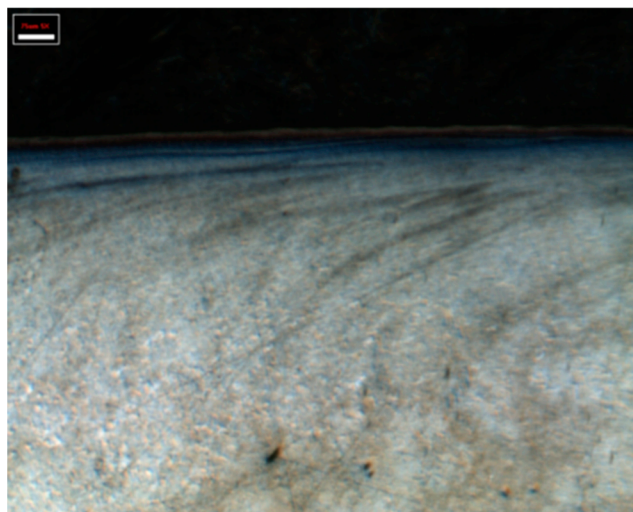


Figure 28. Relationship between residual stress and maximum shear stress.

In the case of full slip, the traction coefficient and the maximum coefficient of friction are equal, i.e.,  $f = \mu$  [37]. When estimating surface cracks using the fatigue index, the maximum shear stress can be used [37]. Since it is difficult to measure the maximum shear stress occurring on the specimen or wheel, the relationship between the maximum shear stress and the residual stress in Equation (7) can be used. Figure 29 shows the plastic deformation of and crack in the rail specimen at the 1.5% slip ratio. In this case, the residual stress was  $-406$  MPa and the maximum shear stress was predicted to be 687 MPa from Equation (7). Assuming that the shear yield strength ( $k$ ) is about 300 MPa [37], the occurrence of surface cracks could be predicted from Equation (5).



**Figure 29.** Plastic flow and crack at slip ratio of 1.5%.

## 5. Conclusions

In this study, the mechanical properties and fatigue characteristics of the two types of wheel and rail were evaluated, and the effects on wear and contact fatigue were examined. The following conclusions were obtained.

(1) The KS60-rail and UIC60-rail appeared to have higher yield strength and hardness with lower elongation compared to those of the RSW-wheel and R7-wheel. The fracture toughness of the KS60-rail was  $73 \text{ MPa}\sqrt{\text{m}}$ , 1.8 times higher than the  $41 \text{ MPa}\sqrt{\text{m}}$  of the UIC60-rail.

(2) The wear resistance of the UIC60-rail and R7-wheel appeared better than that of the KS60-rail and RSW-wheel. The hardness ratios of the two types of test specimens appeared similar to each other; however, the pair of the UIC60-rail and R7-wheel showed a higher wear resistance, owing to its relatively higher total hardness. The evaluation of the wear resistance of a pair of wheel and rail solely by using the hardness ratios of respective materials would be inappropriate; the two factors of the hardness ratio and the total hardness should be taken into account together for an assessment.

(3) The mechanical properties of the tensile strength and hardness of the UIC60-rail appeared better than those of the KS60-rail. However, the contact fatigue life of the UIC60-rail appeared shorter than that of the KS60-rail. This was attributable to the fracture toughness and crack growth rate of the KS60-rail, which were superior to those of the UIC60-rail. Thus, the assessment of contact fatigue life should take the fracture toughness and the crack growth rate into account as well as the mechanical properties of tensile strength and hardness.

(4) The residual stress in the KS60-rail appeared higher than that in the UIC60-rail. This was due to the lower yield strength and larger elongation of the KS60-rail than those of the UIC60-rail. The residual stress in KS60-rail increased proportionally to the maximum shear stress.

**Author Contributions:** Conceptualization, J.-W.S. and H.-M.H.; methodology, J.-W.S. and S.-J.K.; formal analysis, J.-W.S. and H.-M.H.; investigation, H.-M.H. and S.-J.K.; data curation, J.-W.S. and S.-J.K.; writing—original draft preparation, writing—review and editing, J.-W.S., H.-M.H. and S.-J.K.; supervision, J.-W.S.; funding acquisition, H.-M.H. and J.-W.S. All authors have read and agreed to the published version of the manuscript.

**Funding:** This work was supported by a Korea Agency for Infrastructure Technology Advancement (KAIA) grant funded by the Ministry of Land, Infrastructure and Transport (project code: 22CACB-C163504-02, Development of Technology for Commercialization of Active Steering Bogie for Electric Railway Vehicle in a Sharp Curve).

**Data Availability Statement:** Data are contained within the article.

**Conflicts of Interest:** The authors declare no conflict of interest.

## References

1. Krishna, V.; Hossein-Nia, S.; Casanueva, C.; Stichel, S. Long term rail surface damage considering maintenance interventions. *Wear* **2020**, *460–461*, 203462. [[CrossRef](#)]
2. Borja, R.; Albi, S.E.; Unai, A.; Jose, M.M.; Javier, N. Prediction of Rolling Contact Fatigue Behavior in Rails Using Crack Initiation and Growth Models along with Multibody Simulations. *Appl. Sci.* **2021**, *11*, 1026.
3. Lian, Q.; Deng, G.; Zhu, H.; Li, H.; Wang, X.; Liu, Z. Influence of white etching layer on rolling contact behavior at wheel-rail interface. *Friction* **2020**, *8*, 1178–1196. [[CrossRef](#)]
4. Lian, Q.; Zhu, H.; Deng, G.; Wang, X.; Li, H.; Wang, X.; Liu, Z. Evolution of thermally induced white etching layer at rail surface during multiple wheel/train passages. *Int. J. Fatigue* **2022**, *159*, 106799. [[CrossRef](#)]
5. Zhao, X.; An, B.; Zhao, X.; Wen, Z.; Jin, X. Local rolling contact fatigue and indentations on high-speed railway wheels: Observations and numerical simulations. *Int. J. Fatigue* **2017**, *103*, 5–16. [[CrossRef](#)]
6. Zhao, X.; Wang, Z.; Wen, Z.; Wang, H.; Zeng, D. The initiation of local rolling contact fatigue on railway wheels: An experimental study. *Int. J. Fatigue* **2020**, *132*, 105345. [[CrossRef](#)]
7. Tyfour, W.R.; Beynon, J.H.; Kapoor, A. The steady state wear behavior of pearlitic rail steel under dry rolling-sliding contact condition. *Wear* **1995**, *180*, 79–89. [[CrossRef](#)]
8. Lewis, R.; Olofsson, U. Mapping rail wear regimes and transitions. *Wear* **2004**, *257*, 721–729. [[CrossRef](#)]
9. Kondo, K.; Yoroizaka, K.; Sato, Y. Cause, increase, diagnosis, countermeasures and elimination of Shinkansen shelling. *Wear* **1996**, *191*, 199–203. [[CrossRef](#)]
10. Cannon, D.F.; Pradier, H. Rail rolling contact fatigue Research by the European Rail Research Institute. *Wear* **1996**, *191*, 1–13. [[CrossRef](#)]
11. Taizo, M.; Takanori, K.; Kenji, H. The effect of slip ratio on the rolling contact fatigue property of railway wheel steel. *Int. J. Fatigue* **2012**, *36*, 68–79.
12. Zhong, W.; Hu, J.J.; Li, Z.B.; Liu, Z.R.; Zhou, Z.R. A study of rolling contact fatigue crack growth in U75V and U71Mn rails. *Wear* **2011**, *271*, 388–392. [[CrossRef](#)]
13. EN 13674; Railway Applications—Track-Rail. European Committee for Standardization: Brussels, Belgium, 2011.
14. EN 13262; Railway Applications—Wheelsets and Bogies—Wheels—Product Requirements. European Committee for Standardization: Brussels, Belgium, 2011.
15. Razhkovskiy, A.A.; Bunkova, T.G.; Petrakova, A.G.; Gateluk, O.V. Optimization of hardness ratio in rail-wheel friction pair. *J. Frict. Wear* **2015**, *36*, 334–341. [[CrossRef](#)]
16. Wang, W.; Jiang, W.; Wang, H.; Liu, Q.; Zhu, M.; Jin, X. Experimental study on the wear and damage behavior of different wheel/rail materials. *J. Rail Rapid Transit* **2016**, *230*, 3–14. [[CrossRef](#)]
17. Hu, Y.; Zhou, L.; Dong, H.H.; Tan, G.X.; Lewis, R.; Liu, Q.Y.; Guo, J.; Wang, W.J. Investigation on wear and rolling contact fatigue of wheel-rail materials under various wheel/rail hardness ratio and creepage conditions. *Tribol. Int.* **2020**, *143*, 106091. [[CrossRef](#)]
18. Donzella, G.; Faccoli, M.; Ghidini, A. The competitive role of wear and RCF in a rail steel. *Eng. Fract. Mech.* **2005**, *72*, 287–308. [[CrossRef](#)]
19. Donzella, G.; Mazzu, A.; Petrogalli, C. Competition between wear and rolling contact fatigue at the wheel-rail interface: Some experimental evidence on rail steel. *Proc. Inst. Mech. Eng. Part F J. Rail Rapid Transit* **2009**, *223*, 31–44. [[CrossRef](#)]
20. Ishida, M.; Abe, N. Experimental study on rolling contact fatigue from the aspect of residual stress. *Wear* **1996**, *191*, 65–71. [[CrossRef](#)]
21. Batista, A.C.; Peixoto, D.F.C.; Nobre, J.P.; Coelho, L. Wear and surface residual stress evaluation on twin-disc tests of rail/wheel steels. *Mat. Sci. Forum* **2014**, *768–769*, 707–713.
22. Ueda, M.; Matsuda, K. Effects of carbon and hardness on rolling contact fatigue resistance in heavily loaded pearlitic rail steels. *Wear* **2020**, *444–445*, 203120. [[CrossRef](#)]
23. Liu, C.; Zhao, X.; Liu, P.; Pan, J.; Ren, R. Influence of contact stress on surface microstructure and wear property of D2/U71Mn Wheel-Rail Material. *Materials* **2019**, *12*, 3268. [[CrossRef](#)] [[PubMed](#)]

24. Pereira, H.B.; Alves, L.H.D.; Rezende, A.B.; Mei, P.R.; Goldensten, H. Influence of the microstructure on the rolling contact fatigue of rail steel: Spheroidized pearlite and fully pearlitic microstructure analysis. *Wear* **2022**, *498–499*, 204299. [[CrossRef](#)]
25. Li, Q.; Guo, J.; Zhao, A. Effect of upper Bainite on wear behaviour of high-speed wheel steel. *Tribol. Lett.* **2019**, *67*, 121. [[CrossRef](#)]
26. Liu, J.; Li, Y.; Zhang, Y.; Hu, Y.; Shi, L.; Ding, H.; Wang, W.; Liu, F.; Zhou, S.; Shi, T. Dry rolling/sliding wear of bainitic rail steels under different contact stresses and slip ratios. *Materials* **2020**, *13*, 4678. [[CrossRef](#)] [[PubMed](#)]
27. Miranda, R.S.; Rezende, A.B.; Fonseca, S.T.; Fernandes, F.M.; Sinatora, A.; Mei, P.R. Fatigue and wear behavior of pearlitic and bainitic microstructures with the same chemical composition and hardness using twin-disc tests. *Wear* **2022**, *494–495*, 204253. [[CrossRef](#)]
28. Liu, M.; Fan, Y.; Gui, X.; Hu, J.; Wang, X.; Gao, G. Relationship between microstructure and properties of 1308 MPa Grade bainitic rail steel treated by online bainite-based Quenching and partitioning concept. *Metals* **2022**, *12*, 330. [[CrossRef](#)]
29. Pointer, P. High strength rail steels—The importance of material properties in contact mechanics problems. *Wear* **2008**, *265*, 1373–1379. [[CrossRef](#)]
30. Noda, T. Safety of wheels and axles for railway vehicles and engineering ethics. *Forum* **2002**, *7*, 9–16.
31. *ASTM-E647*; Standard test Method for Measurement of Fatigue Crack Growth Rates. ASTM Standards. American Society for Testing and Materials: West Conshohocken, PA, USA, 2001; Volume 3.
32. Tyfour, W.R.; Beynon, J.H.; Kapoor, A. Deterioration of rolling contact fatigue life of pearlitic rail steel due to dry-wet rolling-sliding line contact. *Wear* **1996**, *197*, 255–265. [[CrossRef](#)]
33. Benson, M. *Effect of Differential Hardness on Wheel/Rail Wear Literature Survey*; British Rail Research Report LR MT 0006; British Rail Research Division: Derby, UK, 1993.
34. Zhou, G.Y.; Liu, J.H.; Wang, W.J.; Wen, G.; Liu, Q.Y. Study on the fatigue and wear characteristics of four wheel materials. *J. Mod. Transp.* **2013**, *21*, 182–193. [[CrossRef](#)]
35. Liu, Y.; Stratman, B.; Mahadevan, S. Fatigue crack initiation life prediction of railroad wheels. *Int. J. Fatigue* **2006**, *28*, 747–756. [[CrossRef](#)]
36. Ekberg, A.; Kabo, E.; Andersson, H. An engineering model for prediction of rolling contact fatigue of railway wheels. *Fatigue Fract. Eng. Mater. Struct.* **2002**, *25*, 899–909. [[CrossRef](#)]
37. Ekberg, A.; Paulsson, B. *Innovative Laboratory Tests for Rail Steels*; INNOTRACK D4.3.7 Final Report; International Union of Railways: Paris, France, 2009; pp. 18–21.